

STRUCTURAL INTERPRETATION OF AIRBORNE MAGNETIC SURVEY DATA IN THE KAB AMIRI AREA, CENTRAL EASTERN DESERT, EGYPT

Said I. Rabie, El Sayed M. El Kattan

and

Abuelhoda M. El-Sirafy *

Nuclear Materials Authority
P.O. Box 530 Maadi, Cairo, Egypt

الخلاصة :

تم معالجة البيانات المغناطيسية الجوية لمنطقة (كب عميري) بوسط الصحراء الشرقية - بجمهورية مصر باستخدام تقنيتي حساب زاوية الطور الأفقية والمجال المغناطيسي الأفقي وذلك لتحديد نطاقات التصدع بالمنطقة ، حيث وُجد أن هذه النطاقات تتفق جيدا مع تلك التي رُسمت جيولوجياً أو مع مجاري الوديان الرئيسة شبه المستقيمة .

تم حساب سطحين بينيين متوسطين رئيسيين على عمق (٠٤) و (٠٨) كيلو مترا تحت مستوى القياس وذلك من خلال حساب طيف القدرة المحلي للبيانات المغناطيسية الجوية .

تم تنفيذ ترشيح مصاحب لتحليل المعطيات المغناطيسية الجوية المحولة إلى القطب عند السطحين البينيين المحددين للحصول على أربع خرائط : اثنتان عند كل سطح بيني ، إحداهما للمركبة الاقليمية ، والأخرى للمركبة المتبقية للمجال المغناطيسي . بالإضافة إلى ذلك تم حساب المتجه الأفقي المُقَنَّ والكل عند السطحين البينيين ، وتم رسم أربع خرائط إضافية . وعلاوة على ما تقدم ، تم حساب تغيرات زاويا الطور الأفقية وتم رسم خريطين أخريتين ، أمكن كذلك رسم خريطين تركيبيتين لصخور القاعدة عند السطحين البينيين المحددين وذلك بتكامل المعلومات الناتجة من تطبيق تقنيات التفسير المختلفة .

أظهرت الدراسة وجود عدة مجموعات من نطاقات التصدع تنتمي إلى ست وجهات هي : شمال - جنوب ، شمال شمال الغرب - جنوب جنوب الشرق ، شمال الغرب - جنوب الشرق ، غرب شمال الغرب - شرق جنوب الشرق ، شمال شمال الشرق - جنوب جنوب الشرق ، شمال الشرق - جنوب الغرب .

بناء على هذه النتائج أمكن التوقع أن المنطقة تحت الدراسة تعرضت لقوتي ضغط أساسيتين من إتجاه شرق شمال الشرق (أو شرق - غرب على وجه التقريب) وشمال الشرق .

*To whom correspondence should be addressed.

ABSTRACT

Calculated horizontal phase angle and horizontal magnetic-gradient techniques were applied to aeromagnetic survey data to locate the fault zones in the Kab Amiri area of the Central Eastern Desert of Egypt. These zones correlate well with the faults shown on geological maps.

Two main average interfaces at 0.4 and 0.8 km below the survey flight level were calculated through the computation of the local power spectrum of the aeromagnetic data. Filtering combined with analytical downward continuation of the reduced-to-the-pole (RTP) magnetic map at two interfaces, was also conducted to produce four maps: one for the regional and the other for the residual component of the magnetic field at each interface. In addition, the normalized horizontal and the total vectors gradients maps were computed at the stated interfaces. Moreover, variations of the horizontal phase angles were calculated and additional two maps were prepared. The information obtained from the application of the various methods of interpretation techniques were integrated to construct two basement tectonic maps.

This study revealed the existence of several sets of fault zones trending in six directions: N-S, NNW-SSE, NW-SE, WNW-ESE, NNE-SSE, and NE-SW. Consequently, two maximum principal stresses could be predicted in the area from these results. These are oriented as follows: ENE (or nearly E-W) and NE stresses.

STRUCTURAL INTERPRETATION OF AIRBORNE MAGNETIC SURVEY DATA IN THE KAB AMIRI AREA, CENTRAL EASTERN DESERT, EGYPT

INTRODUCTION

Kab Amiri area is located in the Central Eastern Desert of Egypt (Figure 1), between the River Nile and the Red Sea, and covers a surface area of about 390 km². Topographically, the most notable features in the area include the rugged relief and the highly-dissected Precambrian terrain related to the Red Sea hills.

The airborne magnetic and gamma-ray spectrometric surveys were conducted by the Aeroservice Division of the Western Geophysical Company (U.S.A.) in the area during 1983. These surveys were conducted as the part of the Minerals, Petroleum, and Groundwater Assessment Program (MPGAP).

The aeromagnetic survey was carried out using a Varian V-85 high-sensitivity (0.1 nanotesla) airborne magnetometer with the proton precession sensor being mounted in a tail stinger of a twin engine Cessna Titan, 404 aircraft. The aircraft flew equally-spaced northeast-southwest flight traverses 1.5 km apart at a nominal flight altitude of 120 m ground clearance. Tie lines were flown northwest-southeast at 10 km intervals. The navigation

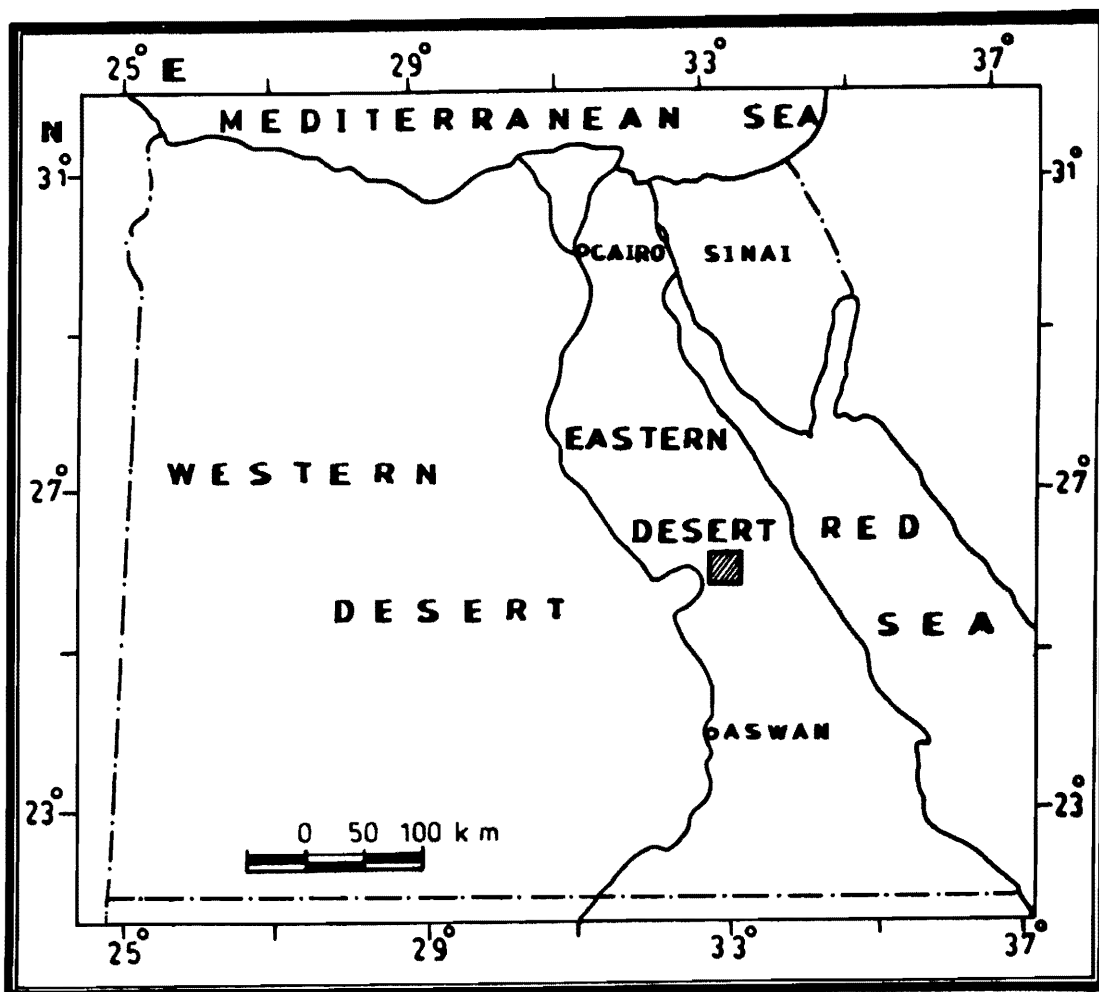


Figure 1. Location Map of Area Under Study.

was controlled using a Bendix Doppler Radar System. A Varian V/W 2321 GA micro processor with a digital and analog recording system was used as a magnetic base station at the base of operations during the survey to correct the magnetic data for the daily variations in the Earth's magnetic field. The aeromagnetic data were reduced, compiled, and presented by Aero-Service in the form of a set of reduced to the pole (RTP) total magnetic-intensity maps at a 1:50,000 scale [1].

GEOLOGICAL OUTLINE

The geological map of the area, compiled from various sources [2–4] is shown in Figure 2. The Kab Amiri area is underlain by basement complex rocks of Precambrian age. These rocks includes five main types, according to El Shazly's classification [5–7]. These are described as follows (from base to top):

Geosynclinal Sediments

These sediments consist mainly of metamudstones, slates, greywackes, schists, and phyllites, that have been subjected to low to moderate-grade metamorphism and to folding [5, 7, 8]. They are represented in this area by quartzite, metamudstone, and, rarely, by metagreywacke [4].

Main Geosynclinal Volcanics

The main geosynclinal volcanics in the area are represented by acidic, intermediate, basic, and ultrabasic volcanics. They are well developed in association with the geosynclinal sediments. They are generally observed interbedded with the geosynclinal sediments in such a way that both of them acquire the same tectonic trend. Contacts between these different metamorphosed volcanics as well as between them and the interbedded geosynclinal sediments are gradational [4].

Synorogenic Plutonites

Synorogenic plutonites in the area are represented mainly by quartz diorite, diorite of epidiorite complex, granodiorite, and grey granite.

Late Orogenic Plutonites

These plutonites are mainly represented by red and pink granites, which possess sharp contacts [9]. Pegmatites occur as veinlets invading the diorite and epidiorites complex [4]. The red and pink granites are best represented in Jabal Kab Amiri and cover a relatively wide part of the area.

Postorogenic Volcanics

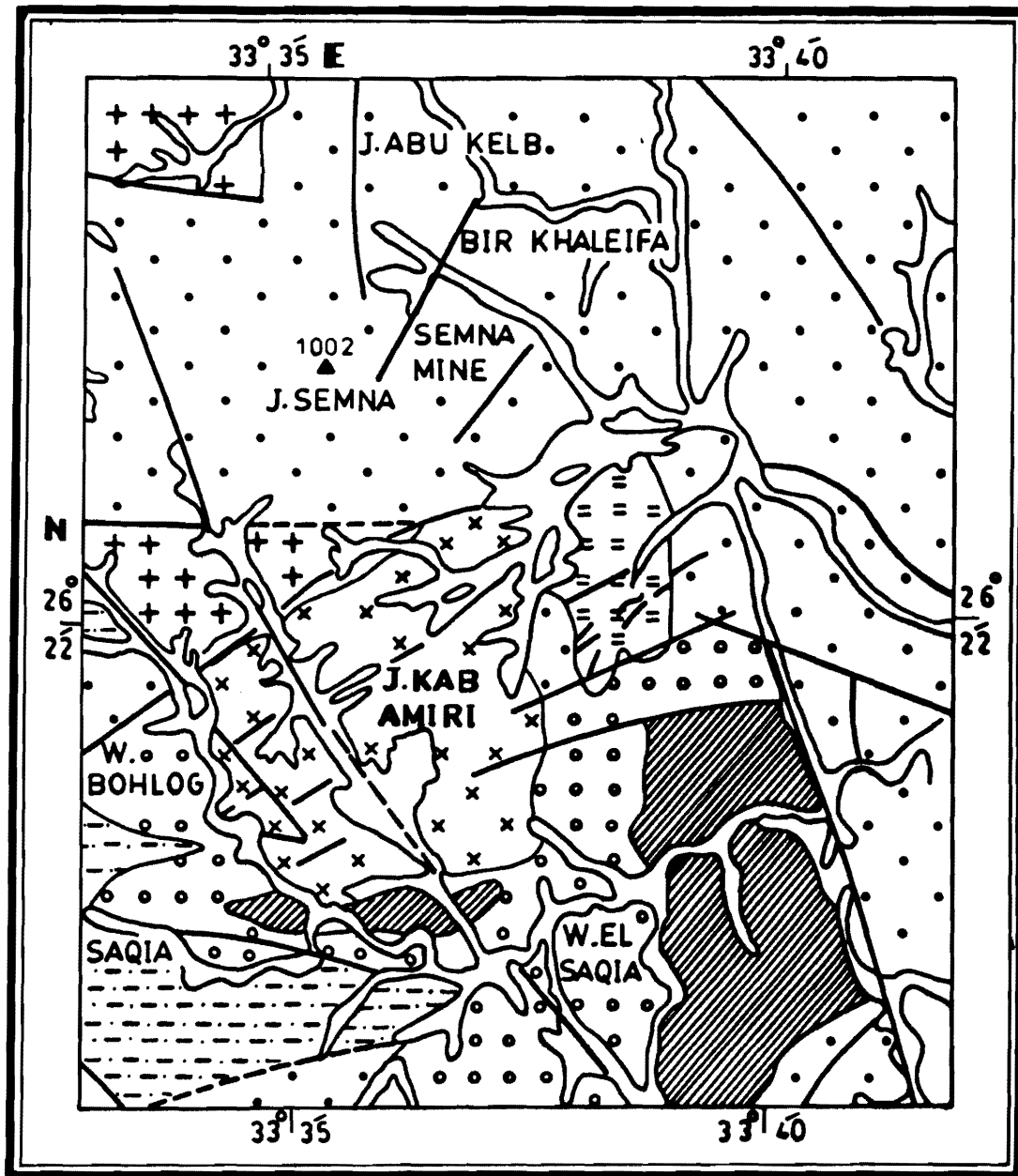
These are widely distributed in the basement cutting the previously-mentioned formation, but not the exposed sedimentary cover. They are generally referred to as post-granite dykes. The main dyke varieties of this group are: andesites, trachytes, and bostonites [5, 7].

INTERPRETATION TECHNIQUES

Calculation of Power Spectrum for Interface Determination

The aeromagnetic data (Figure 3) were analyzed by means of a local power spectrum technique [10]. The restrictions of the procedure were avoided, as considered by Cianciara and Marcak [11].

Two main levels (interfaces) at depth of 0.4 and 0.8 km below the measuring level were interpreted from the average slope of power spectra (Figure 4) on the RTP aeromagnetic survey data.



LEGEND

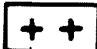


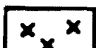
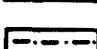
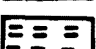


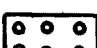


- | | | | |
|---|--------------------------------------|---|---------------------------------|
|  | Granitized Rocks |  | Wadi Deposits |
|  | Acidic to Intermediate Metavolcanics |  | Late Orogenic Plutonites |
|  | Basic to Intermediate Metavolcanics |  | Synorogenic Plutonites |
|  | Metamudstones, Schists |  | Serpentinites and Related Rocks |
|  | Geologic Boundary |  | Fracture and /or Fault |
| | |  | Triangulation Point |

Figure 2. Geological Map of Jabal Kab Amiri Area, Central Eastern Desert, Egypt.

Filtering Combined with Analytical Downward Continuation

Filtering of the RTP magnetic data was carried out using the analytical downward continuation technique described by Cianciara and Marcak [12].

Normalized Horizontal and Total Vector of Field Intensity

To represent the distribution of isolines for the magnitude of the horizontal and the total field vector, the horizontal and total magnetic gradients of magnetic field intensity were, calculated at the two interfaces at depth of 0.4 and 0.8 km respectively.

Horizontal Phase Angle

The horizontal phase angle between the horizontal and vertical components of the total magnetic vector has a very particular property. It transforms the measured data into a new set, so that the portion of data structure accounting for spatial extension of the anomaly source, is amplified [13], whereas the portion connected with source concentration is suppressed.

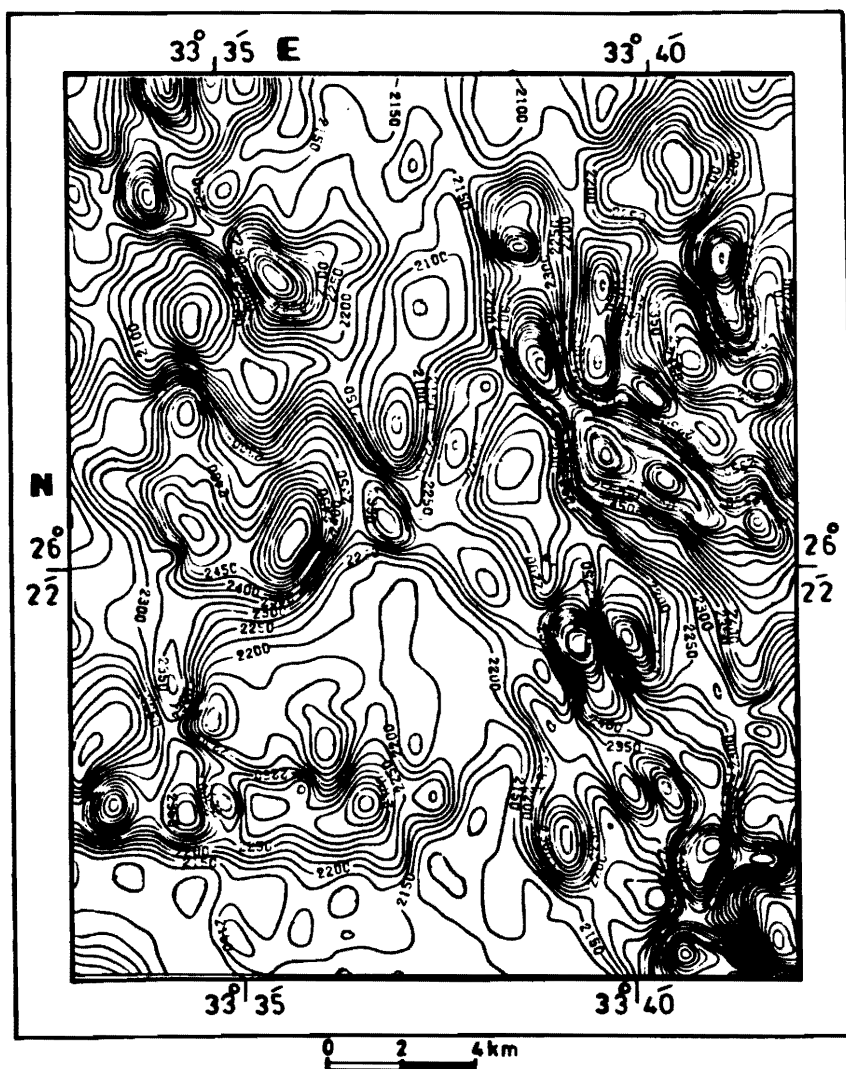


Figure 3. Total Intensity Aeromagnetic Map Reduced to the North Magnetic Pole (RTP), Kab Amiri Area, Central Eastern Desert, Egypt. (Datum removed 40 000 nT; contour interval 25 nT).

The phase angle of ΔT vector is expressed by:

$$F_i = \arctan \frac{H(z)}{Z(z)}$$

where $H(z)$ is the horizontal component of the total magnetic vector and $Z(z)$ is its vertical component.

The phase calculations for magnetic maps provide the possibility to bring out the elongated parts of the map structure and to sharpen them, so that the values with the greatest variations are along lines perpendicular to the strike of the source.

Autocovariance Functions

Autocorrelation functions are applied to aeromagnetic maps to obtain the trend directions which are representative of the geologic structures causing the magnetic anomalies. These functions yield a statistical average of all the magnetic anomalies of an aeromagnetic map, and can be used to interpret stress patterns [14 and 15].

QUALITATIVE INTERPRETATION

The observed magnetic patterns on the magnetic contour maps of the area are a reflection of the contrasts between the magnetic properties of the underlying rocks [16]. Following bands of steep gradient across the map and distinct types of magnetic features, it is possible to delineate the boundaries of the major rock units [17]. According to Parasins [18], the most important feature in the interpretation of aeromagnetic maps is the "texture"

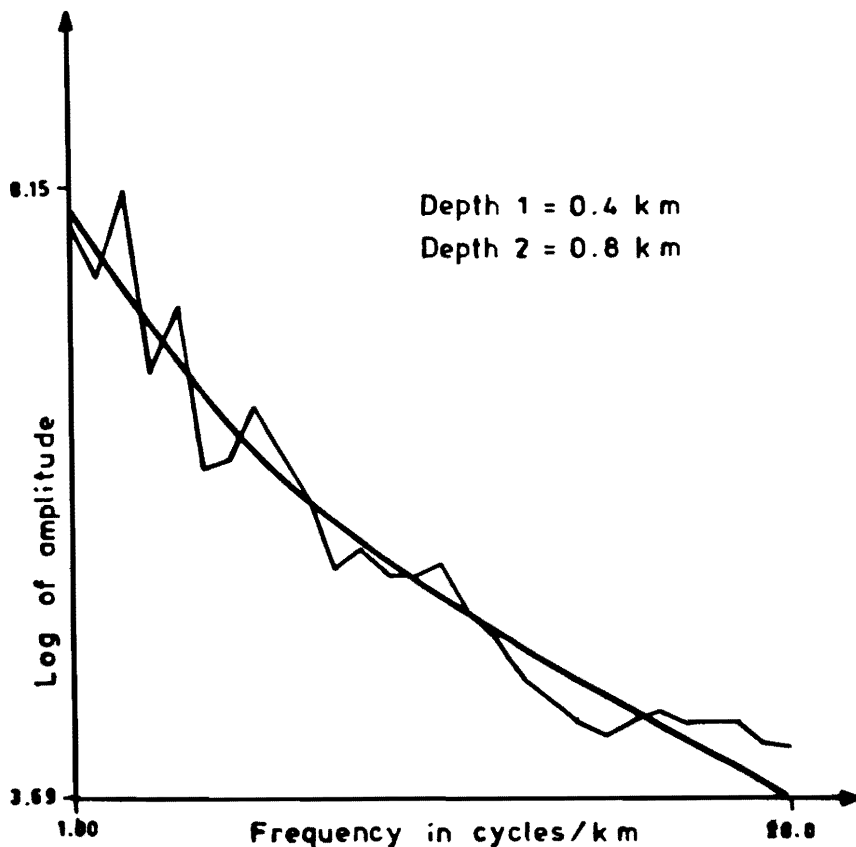


Figure 4. Local Power Spectrum for Interface Determination of Kab Amiri Area, Central Eastern Desert, Egypt.

of the anomaly field. This includes the trends, sizes, and configurations of the various anomaly centers and the occurrence of sharp gradients, *etc.* The boundary between two formations of weakly and highly magnetic properties is recognized on the map from the crowding of magnetic contours along its edge, *i.e.*, from the sharp gradient in the field intensity [18].

The pink granite of Jabal Kab Amiri is located in the south portion of the study area. It is represented by a coarse pink granite with little ferromagnesian mineral content in the southern part, pink granite with ferromagnesian minerals in the center, and pink granite with relatively abundant ferromagnesian minerals in the north. Basic dykes were observed to cross the central and northern parts of the granite complex [2].

The aerial magnetic pattern recorded over the granite complex is relatively simple and remarkably uniform (Figure 3). It is noticeable that the lower magnetic field extends to the east and is considerably larger in areal extent than the one shown in the geological map (Figure 2). Therefore, it is most probable that the eastern extension of these granites has not been exposed by erosional processes. Consequently located at a shallow depth under the surrounding units of main geosynclinal volcanics beyond the eastern contacts of this intrusion with the country rocks.

The complex pink granite unit of Kab Amiri is characterized by relatively lower magnetization and is surrounded by metavolcanic rocks with a much higher magnetization.

The rest of the area is mainly underlain by metavolcanics. The character of the magnetic field recorded over this rock group is quite different from that recorded over the other rock groups. Sometimes, the magnetic pattern is represented by clusters of local and intense anomalies or it may be a flat and featureless calm without anomalies.

The RTP map (Figure 3) shows also a relatively narrow distinct system of linear magnetic anomalies striking nearly NW–SE, parallel to the Red Sea. This character of the magnetic anomalies may correspond to the existence of basic dykes of considerable dimensions intruded along weak tectonic zones [19].

The RTP map (Figure 3) was compiled to present (*a*) the magnetic effects of the magnetized materials near ground level; and (*b*) the magnetic effects of deeply-buried magnetized materials. The two magnetic component maps were interpreted in terms of the lithology and structure. Deep major structures could be resolved and interpreted through the regional magnetic-component map. Two main average interfaces at depths of 0.4 and 0.8 km below the measuring level were revealed through the application of power spectra (Figure 4) on the aeromagnetic map reduced to the north magnetic pole (Figure 3). Four maps were drawn (Figures 5 and 6): two at each interface: one for the residual and the other for the regional magnetic component, respectively.

The residual or near-surface magnetic-component maps (Figure 5) at the two specified levels show a great similarity to the RTP map (Figure 3). This may be due to the fact that most of the basement rocks responsible for the magnetization in the area either outcrop or else are buried at shallow depth. The two residual maps show relatively-elongated high magnetic anomalies trending in approximately NW–SE direction, and associated with the deep-seated basic dykes intruded in the weak zones.

The regional or deep-seated magnetic component maps (Figure 6) at the two interfaces are the result of the removal of the anomalies corresponding to the intrusives from the recorded (RTP) aeromagnetic anomalies. These maps show approximately NW–SE and N–S trending axes of the anomalous zones possessing relatively a high magnetization. They, also indicate relatively weaker magnetization of the granitic rocks located to the south of the area, corresponding to Kab Amiri younger granite. This relatively low amplitude and frequency magnetic anomaly associates with granites is surrounded on all sides by anomalies having relatively high magnetic character, indicative of metavolcanics and other rocks.

Figures 7 and 8 represent the horizontal and total vector gradients at the two interfaces. The horizontal and the total gradient maps show pattern of anomalies that are related to the real sources at each interface. Besides, it was possible from the total horizontal vector maps to delineate structural features such as faulting and folding. The closures having the highest values in the middle were interpreted as uplifted blocks (or horsts?), whereas the

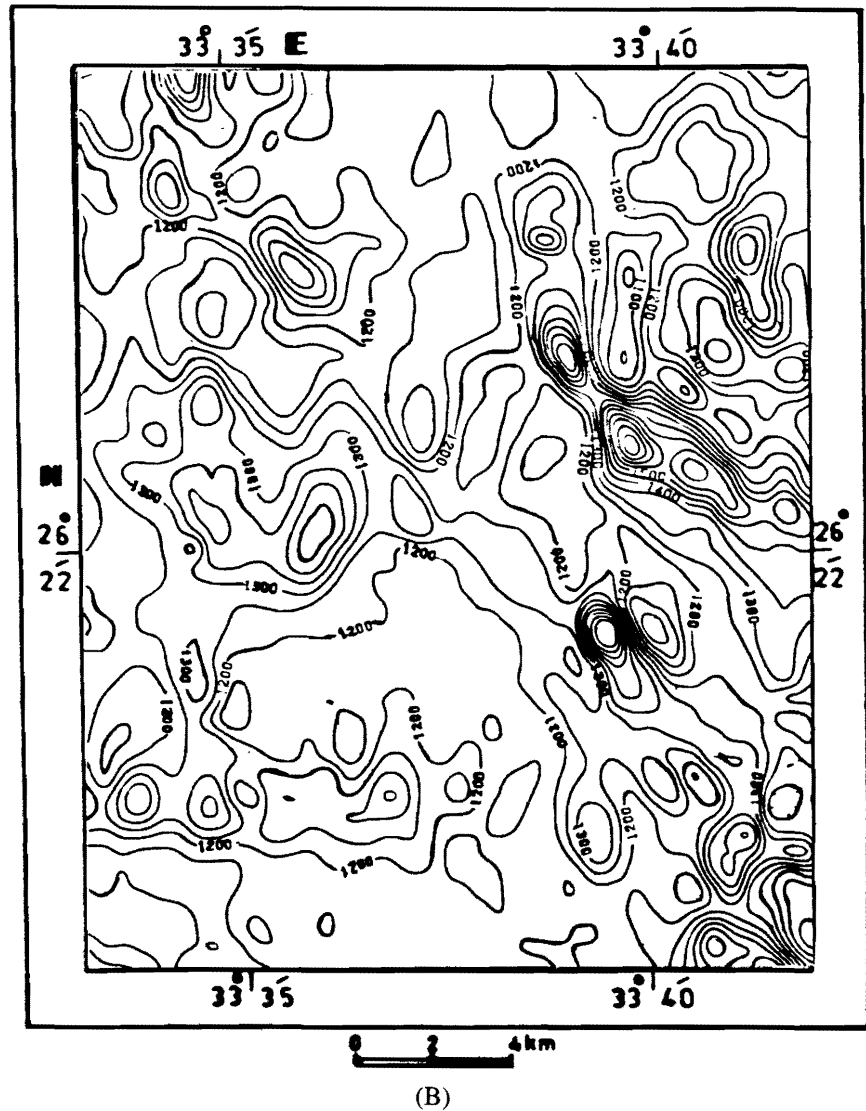
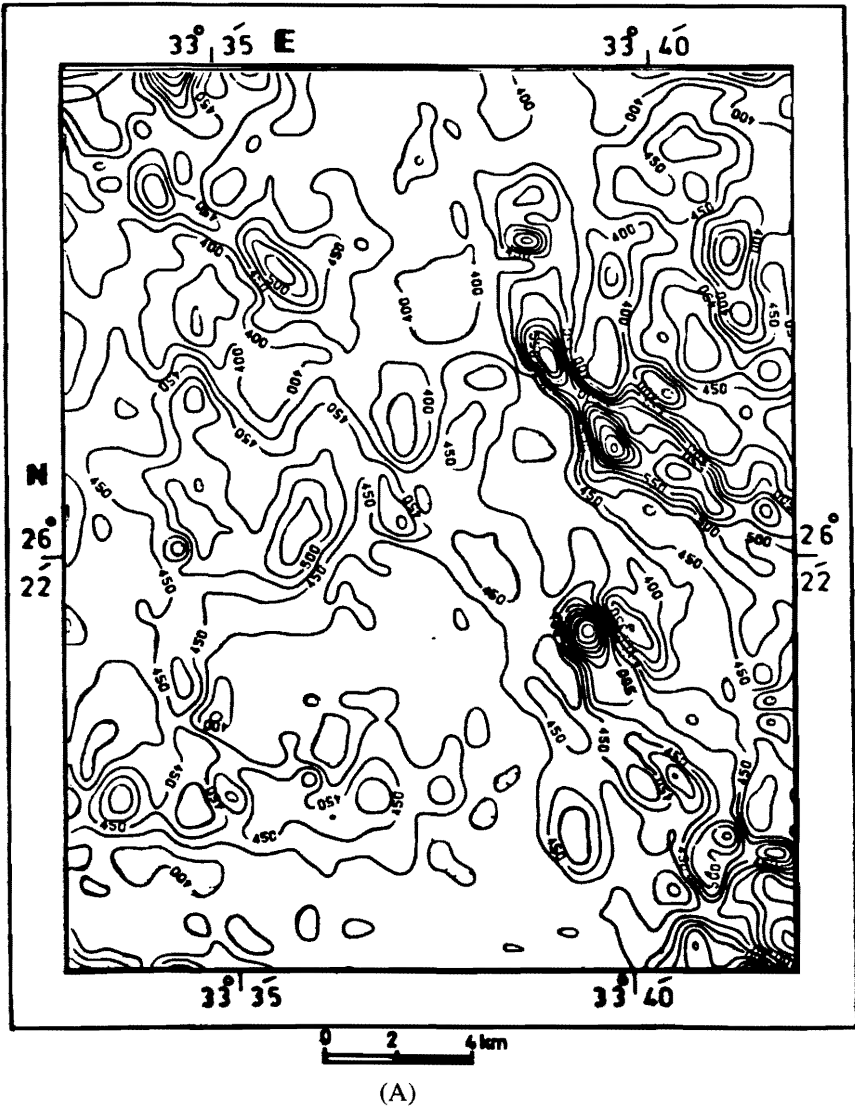


Figure 5. Residual Magnetic-Component Maps at Interfaces 0.4 km (A) and 0.8 km (B), Kab Amiri Area, Central Eastern Desert, Egypt. (Contour interval 50 nT).

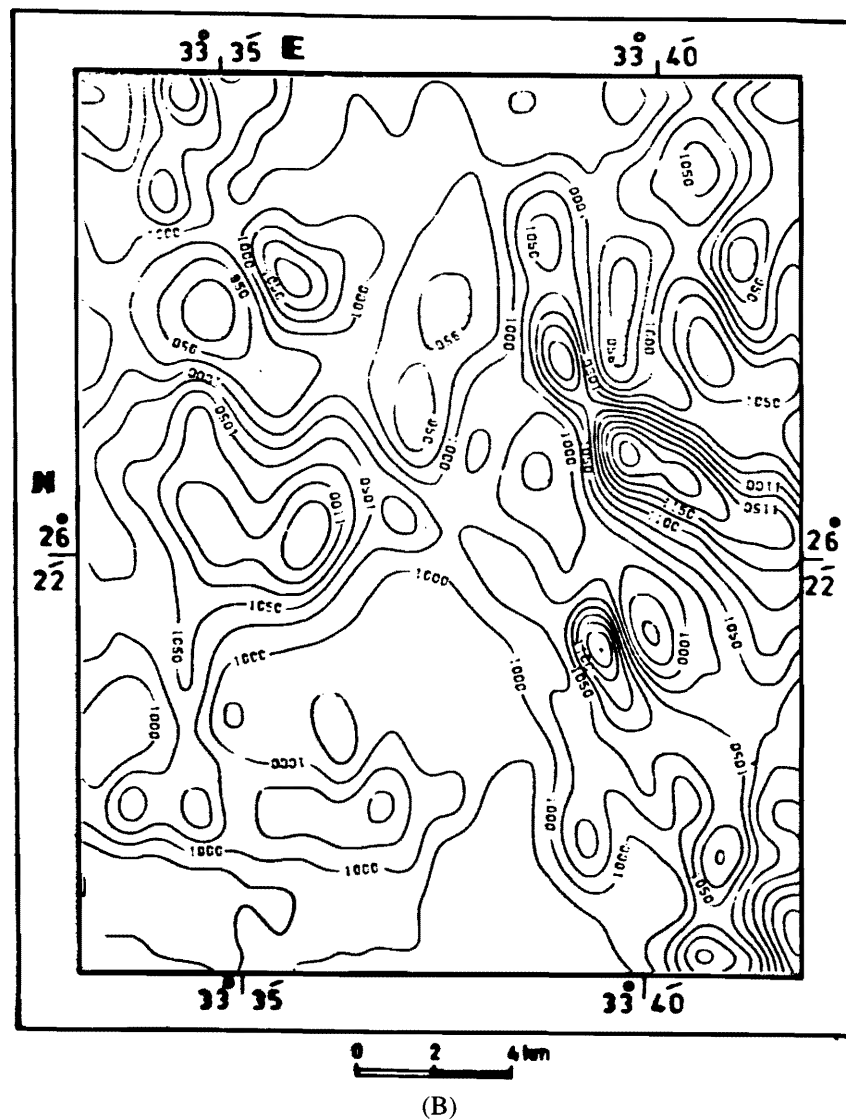
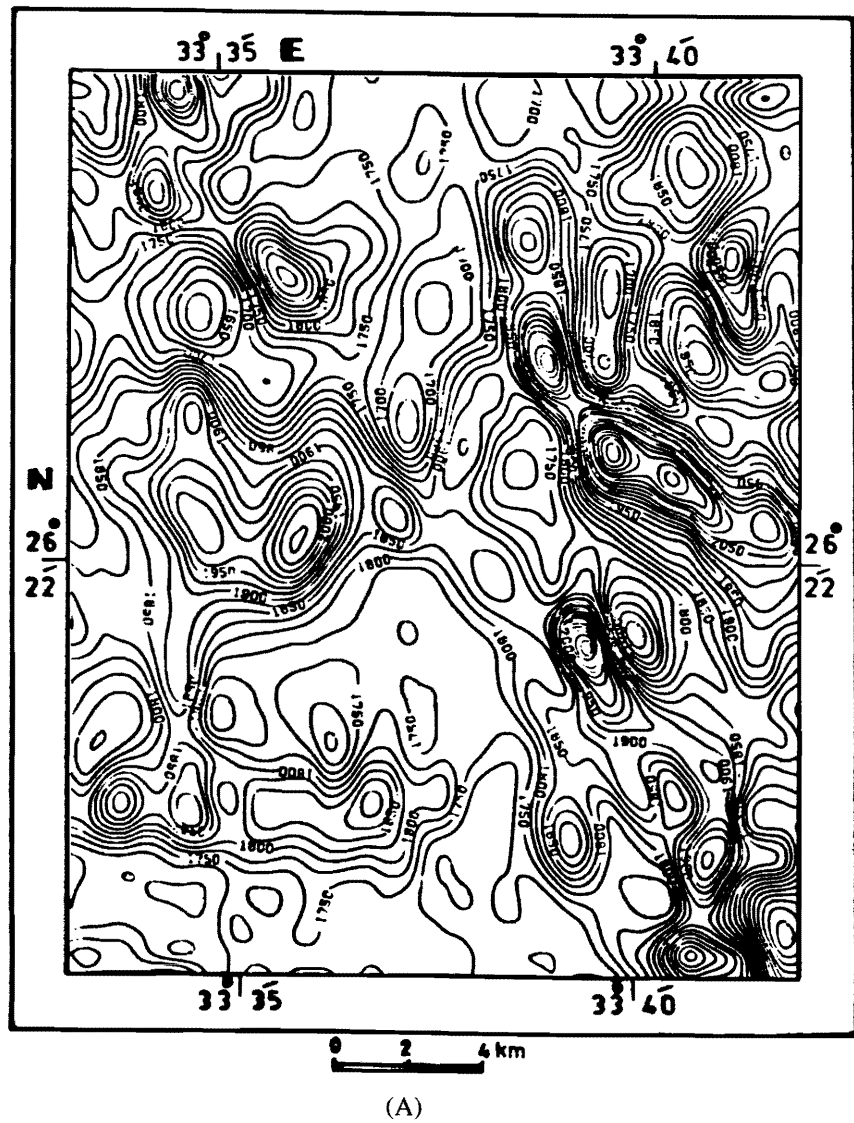
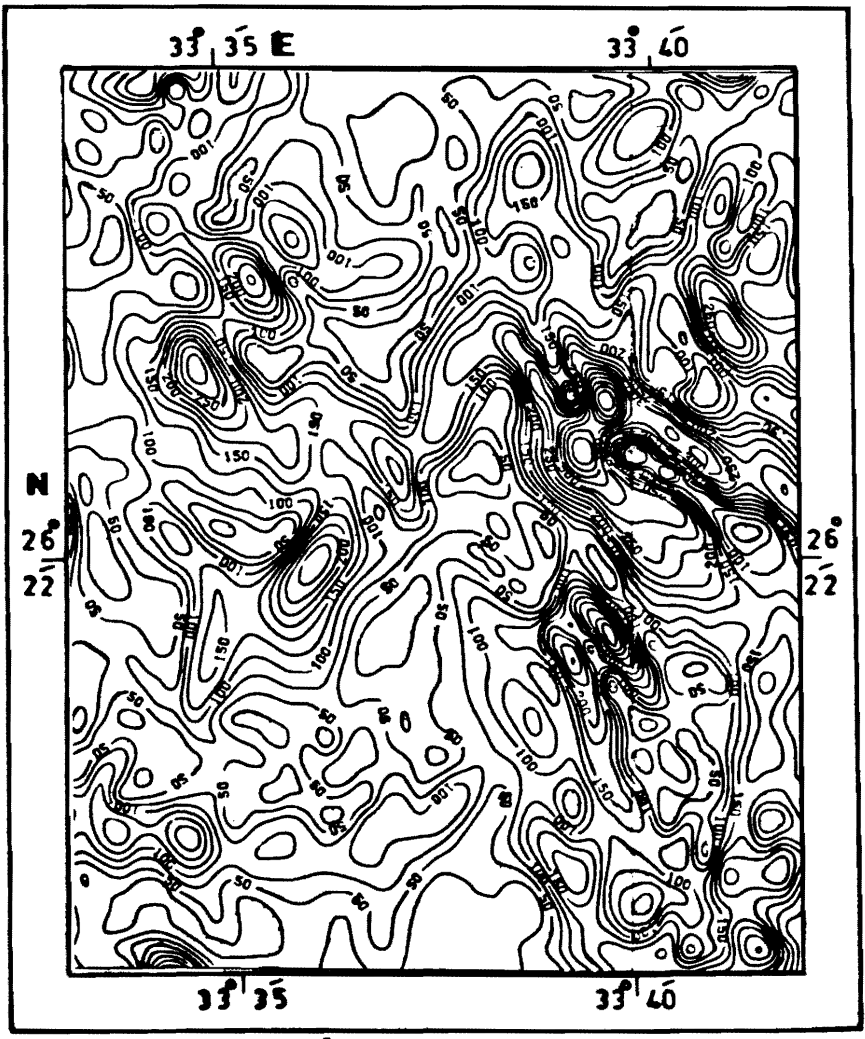
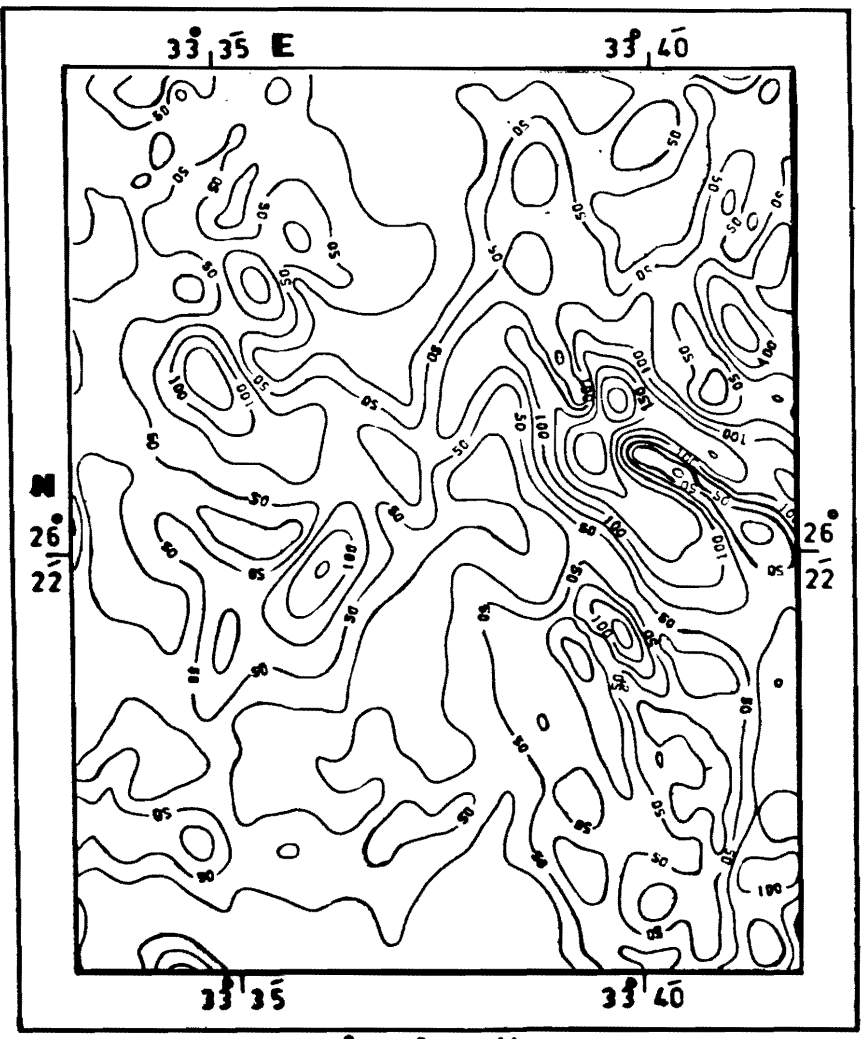


Figure 6. Regional Magnetic-Component Maps at Interfaces 0.4 km (A) and 0.8 km (B), Kab Amiri Area, Central Eastern Desert, Egypt. (Contour interval 25 nT).



(A)



(B)

Figure 7. Horizontal Magnetic Vector Maps at Interfaces 0.4 km (A) and 0.8 km (B), Kab Amiri Area, Central Eastern Desert, Egypt.

S. I. Rabie, S. M. El Kattan, and A. M. El-Sirafy

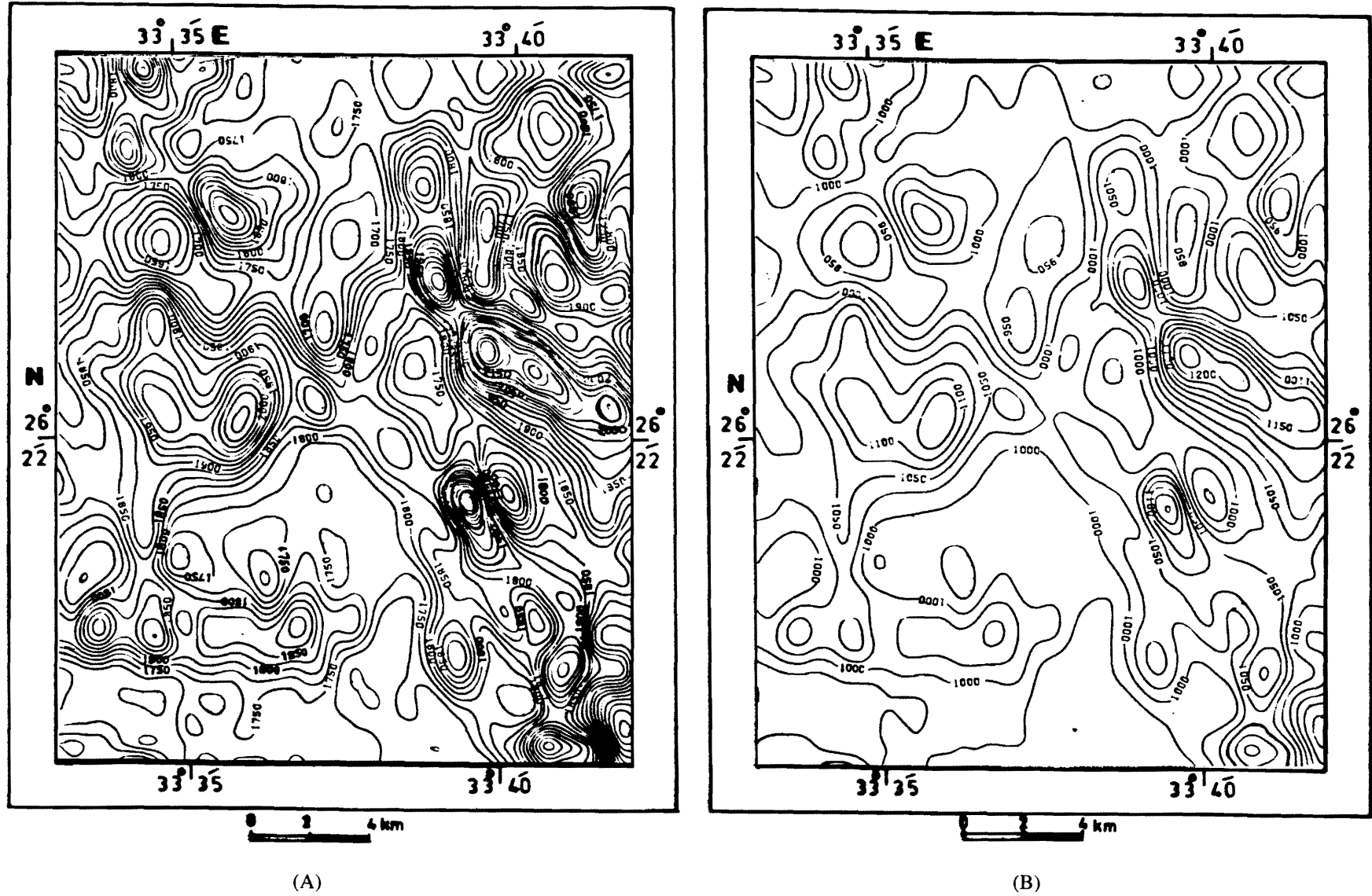
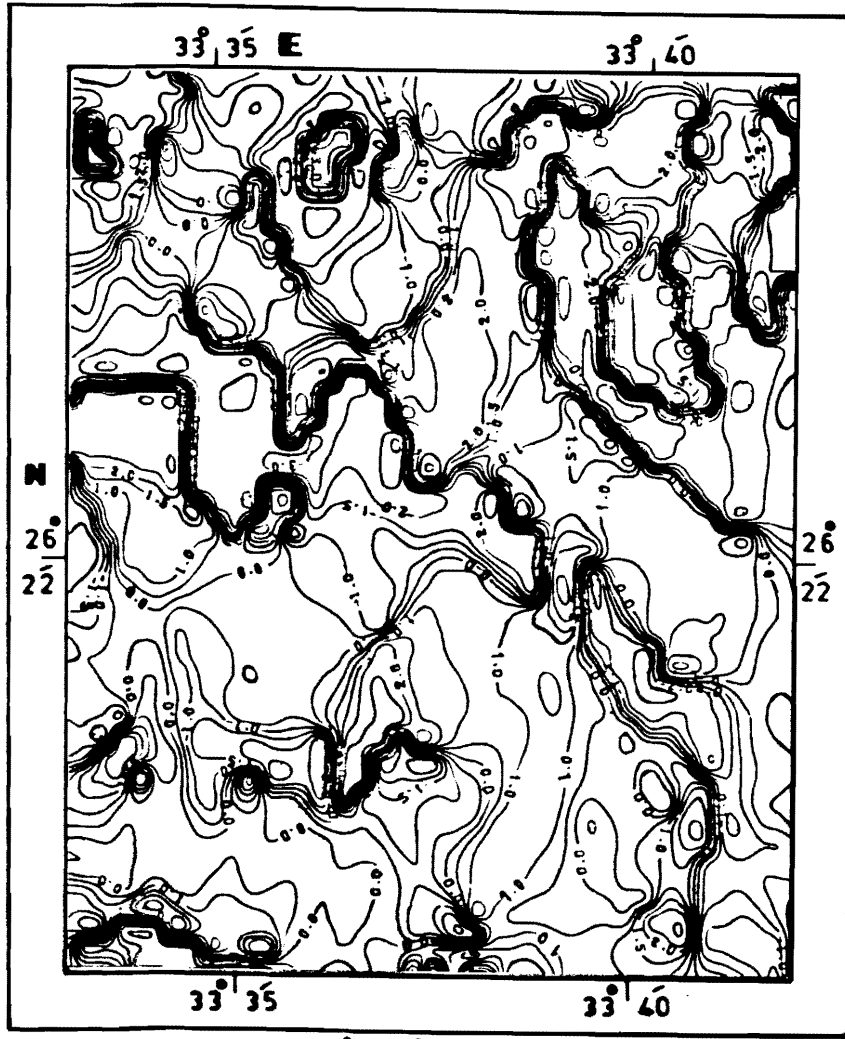
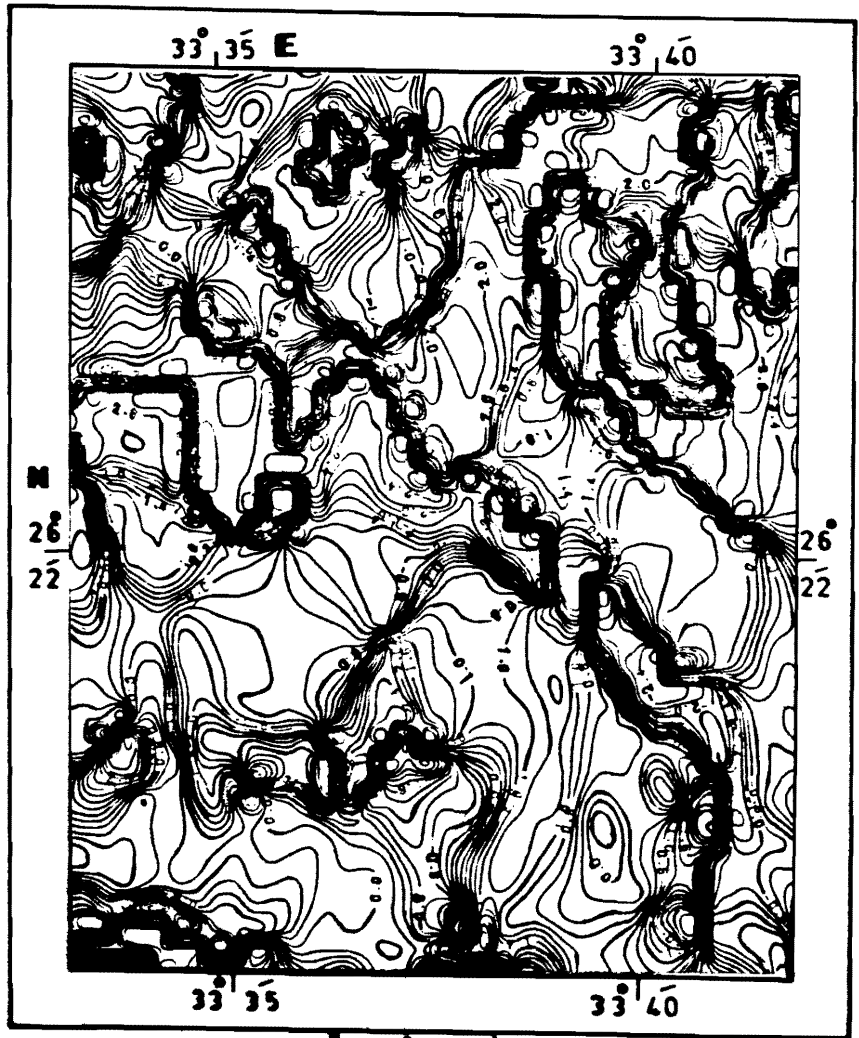


Figure 8. Total Magnetic Vector Maps at Interfaces 0.4 km (A) and 0.8 km (B), Kab Amiri Area, Central Eastern Desert, Egypt.



(A)



(B)

Figure 9. Horizontal Phase Angle Maps at Interfaces 0.4 km (A) and 0.8 km (B), Kab Amiri Area, Central Eastern Desert, Egypt.

closure possessing the lowest values in the middle were interpreted as subsided blocks (or grabens?). The axes of these blocks were correlated with the elongation of the sources.

Figure 9 shows the variation in the computed horizontal phase angle at the two interfaces. It was possible to exactly locate faults, fault zones as well as the extension of bodies having the same magnetic characteristics. The horizontal phase angle shows both the variation in magnetic susceptibility data and the variation in density contrast for the gravity data.

Figure 10 shows the fault zones as interpreted from the horizontal phase angle at the two interfaces. The majority of these fault zones were proved to exist by field check. This technique furnishes a powerful tool in locating the fault zones from the potential field data.

QUANTITATIVE INTERPRETATION

Techniques of analysis of anomaly trends (autocovariance function) for the area were carried out to reveal the structural features from the aeromagnetic data. The correspondence and correlation between the various trends, as well as any significant relation that reflects the control of mineralization are discussed hereafter.

The discussion of the various anomaly trend directions (Figures 11 to 18) as determined from the autocorrelograms, will be based mainly on the suggested geometrical classification of the trend directions [13], consistent with the terminology of the tectonic trends in NE Africa and Arabia. The results of the analyses of major and minor magnetic trends interpreted from various data are summarized in Table 1. These trends are discussed in the following paragraphs.

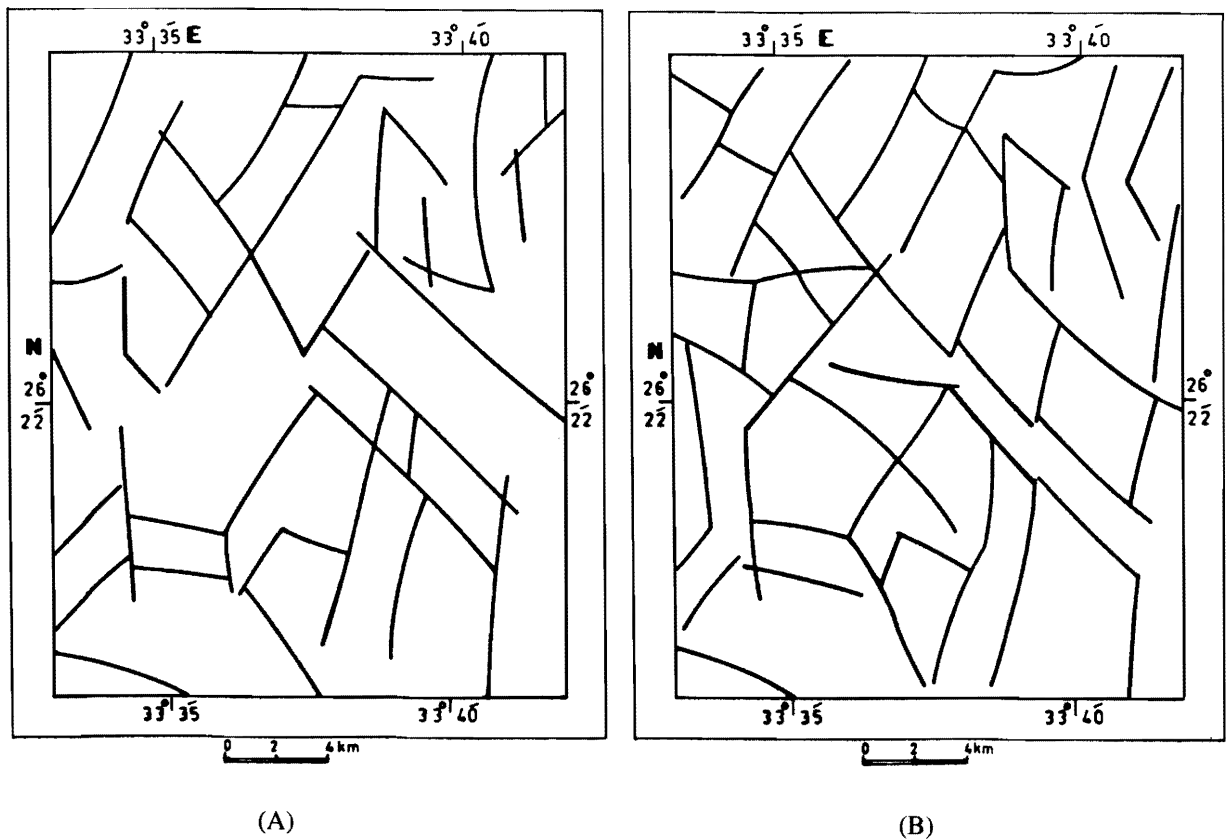


Figure 10. Fault Zones Interpreted from Phase Angle at Interfaces 0.4 km (A) and 0.8 km (B), Kab Amiri Area, Central Eastern Desert, Egypt.

North–South Trend

This trend was registered as the main direction from the residual and regional magnetic component maps at interface 0.8 km, as well as the total magnetic gradient map at interface 0.4 km (Figures 12, 14, and 17). This trend might be considered relatively deep-seated and still effective.

Ammar [20], mentioned that the N–S structures were only observed over the Precambrian basement rocks and did not affect clearly the cover of the Phanerozoic sediments. Ghanem [9] has concluded that the N–S trend had been developed after the emplacement of the late Orogenic Plutonites.

Table 1. Summary of the Principal (Major) and Secondary (Minor) Trend Directions from the Application of Autocovariance Function on the Various Magnetic Data, Kab Amiri Area, Central Eastern Desert, Egypt.

Total Direction	N–S		NNW		Suez Gulf		Najd		Aqaba		Trans-African	
	P	S	P	S	P	S	P	S	P	S	P	S
Residual magnetic component map at 0.4 km			N12°W				N60°W				N53°E	
Residual magnetic component map at 0.8 km	N9°W						N59°W				N50°E	
Regional magnetic component map at 0.4 km		N16°W					N59°W				N44°E	
Regional magnetic component map at 0.8 km	N9°W						N60°W				N42°E	
Horizontal magnetic vector at 0.4 km									N51°W	N15°W	N55°E	
Horizontal magnetic vector at 0.8 km									N49°W	N12°W	N56°E	
Total magnetic vector at 0.4 km	N6°W						N60°W				N47°E	
Total magnetic vector at 0.8 km		N16°W					N61°W				N41°E	

P = Principal trend, S = Secondary trend

NNW-SSE Trend

This trend was developed as the main direction from the residual and regional magnetic component maps at the interface at 0.4 km (Figures 11 and 13), as well as the total magnetic gradient at interface 0.8 km (Figure 18). Consequently, it might be due to relatively deep-seated as well as near-surface structures.

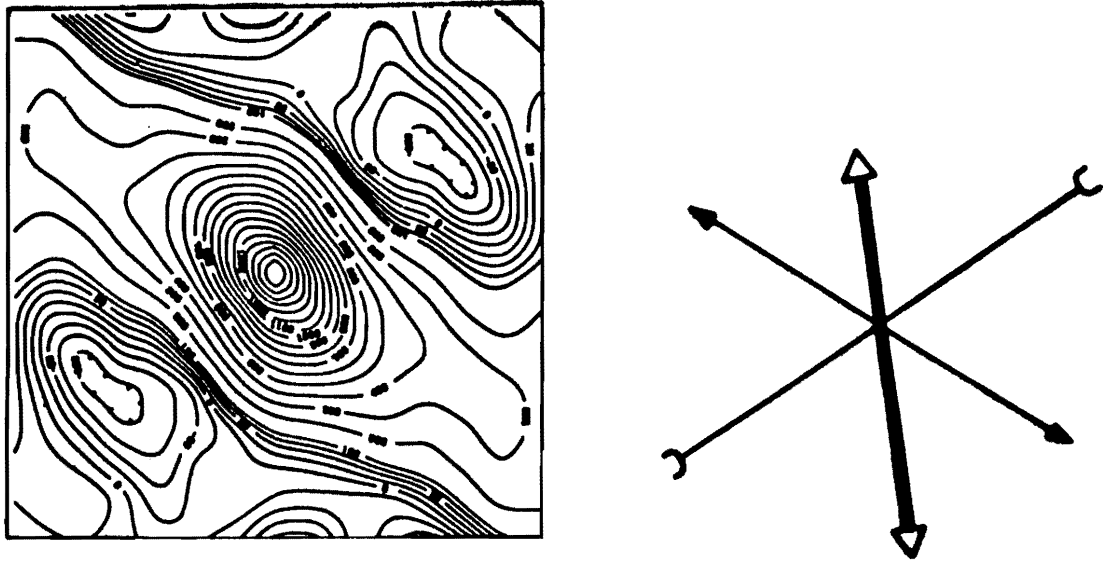


Figure 11. Trend Direction Determined from the Autocorrelogram of the Residual Magnetic Component Map at Interface 0.4 km.

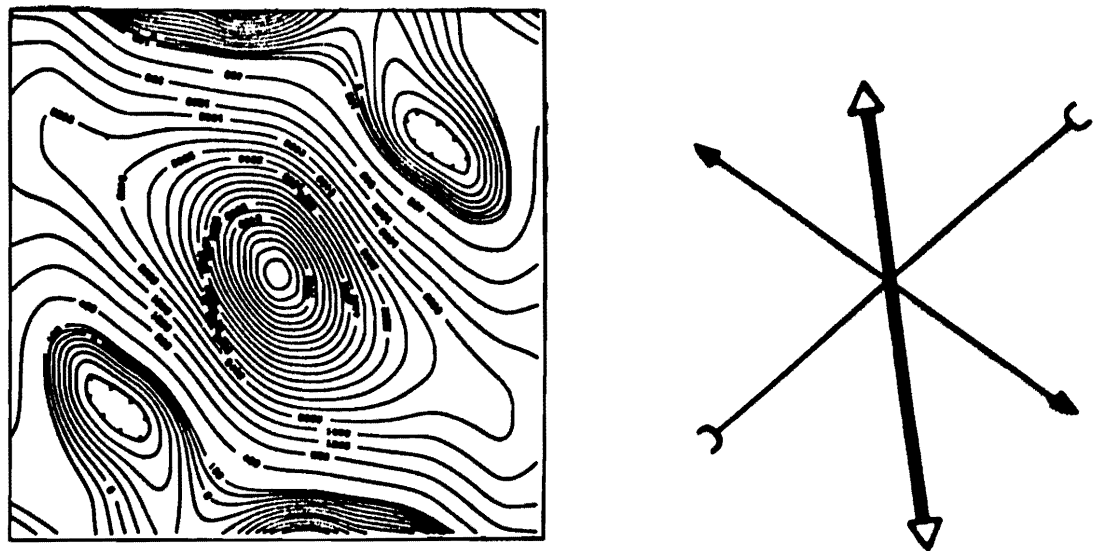


Figure 12. Trend Direction Determined from the Autocorrelogram of the Residual Magnetic Component Map at Interface 0.8 km.

Gulf of Suez–Red Sea NW–SE Trend

This trend was developed as the main direction from the horizontal magnetic vector at the two interfaces of 0.4 and 0.8 km (Figures 15 and 16). It could, therefore, represent an old structure. The interpretation of the Bouguer anomaly map of the northern Egypt by Riad [21], has revealed the presence of almost parallel shears striking in a NW–SE direction. These are probably related to the interaction of the European and African plates.

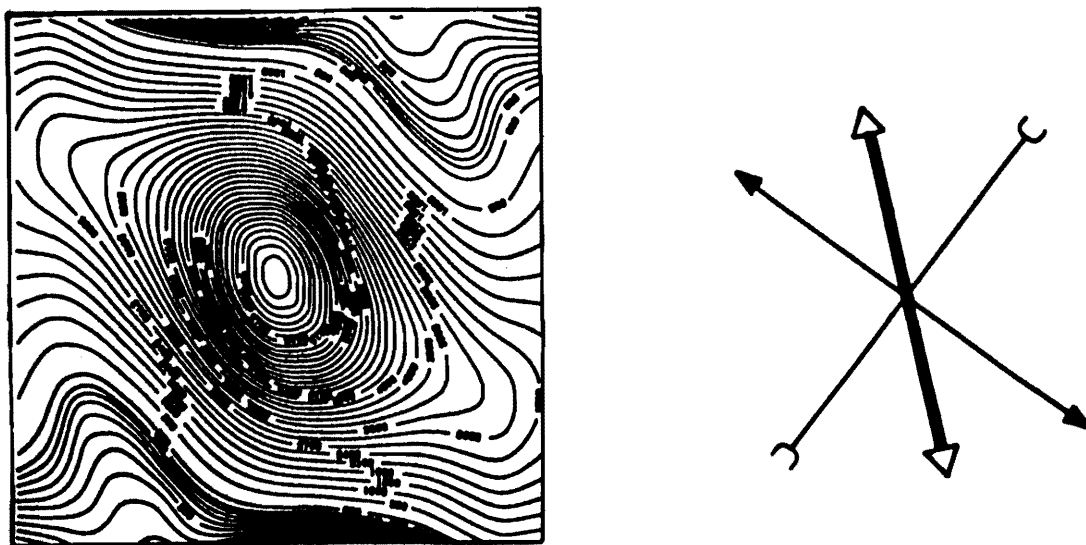


Figure 13. Trend Direction Determined from the Autocorrelogram of the Regional Magnetic Component Map at Interface 0.4 km.

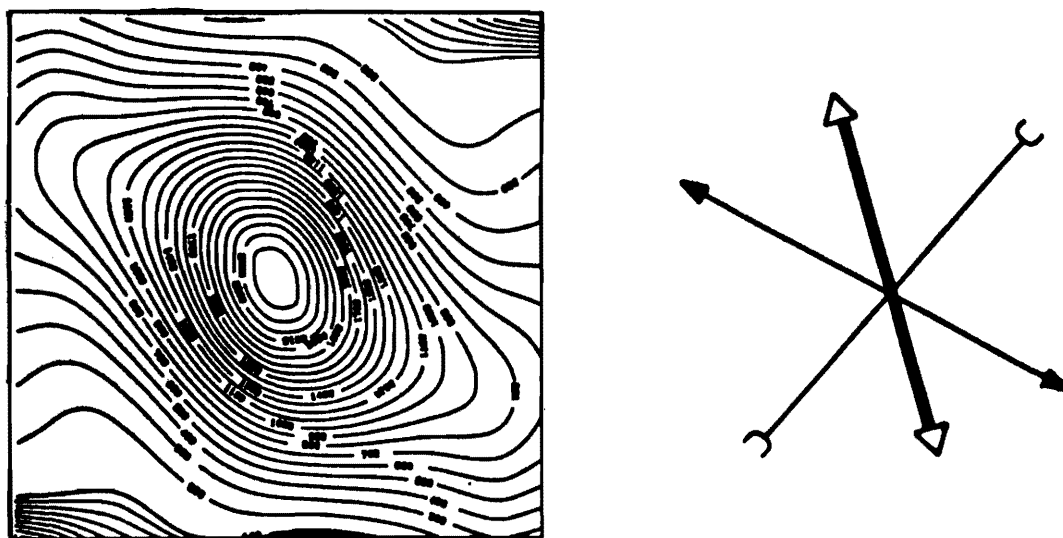


Figure 14. Trend Direction Determined from the Autocorrelogram of the Regional Magnetic Component Map at Interface 0.8 km.

Najd WNW–ESE Trend

This trend was revealed as a minor trend on all magnetic maps except the horizontal magnetic vector at two interfaces (Figures 15 and 16). Consequently, it could represent a near-surface and deep-seated trend that affected the Precambrian basement. According to Gawad [22], it corresponds to the lineaments in the overlying sediments in the Gulf of Suez and Red Sea region. Dynamically, the N 65°W trend was interpreted to be due to the shear couple that affected the Red Sea region [23]. Therefore, an evident relationship could be clearly observed between this trend and the Gulf of Suez–Red Sea trend.

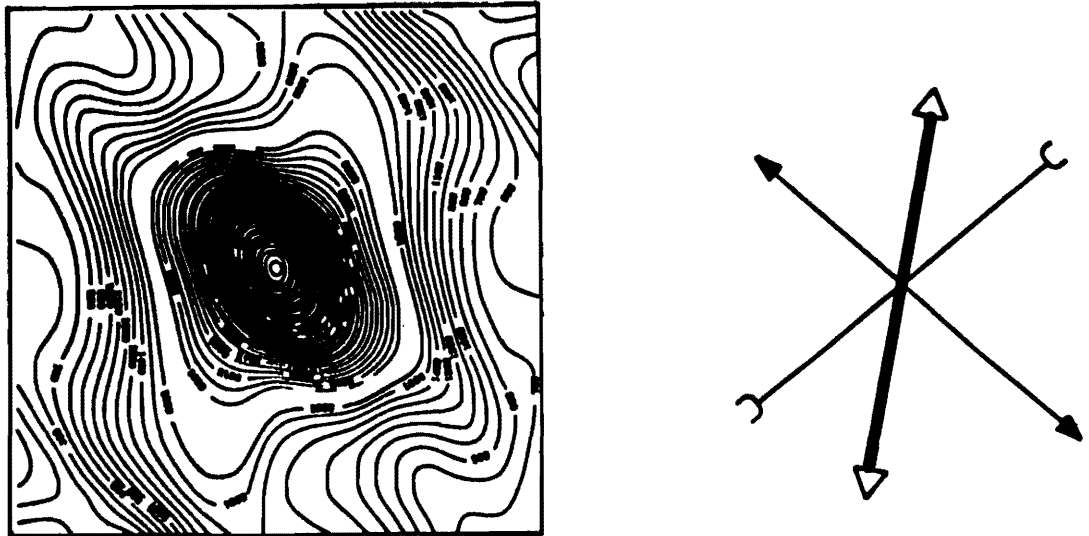


Figure 15. Trend Direction Determined from the Autocorrelogram of the Horizontal Magnetic Vector Map at Interface 0.4 km.

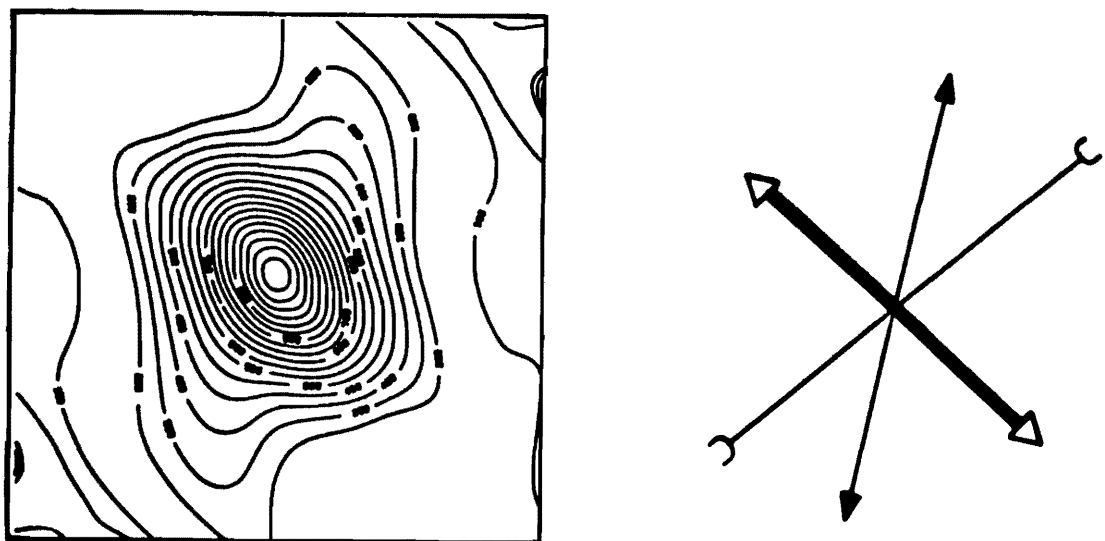


Figure 16. Trend Direction Determined from the Autocorrelogram of the Horizontal Magnetic Vector Map at Interface 0.8 km.

Aqaba NNE-SSW Trend

This trend was developed as a minor trend from the two autocorrelograms of the horizontal magnetic vector at the two interfaces of 0.4 and 0.8 km (Figures 15 and 16).

Meshref [24] interpreted this trend and the NW-SE trend to represent the two vertical shear fractures resulting from the northern compression which was active by the end of the mountain building stage and postorogenic transitional stage. Dynamically, the Aqaba trend is the left lateral component of the conjugate shear pattern of which the Suez direction is the more prominent member [25].

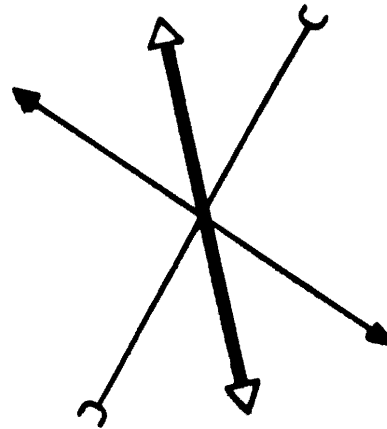
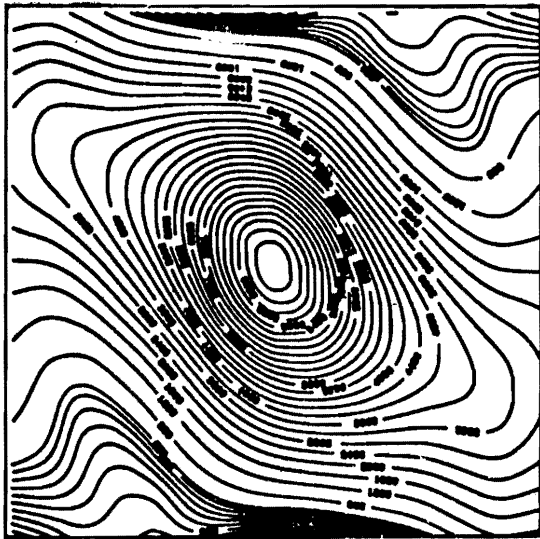


Figure 17. Trend Direction Determined from the Autocorrelogram of the Total Magnetic Vector Map at Interface 0.4 km.

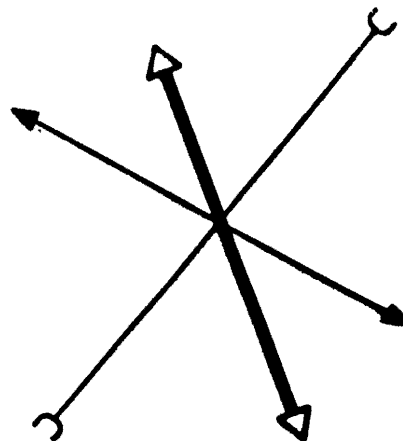
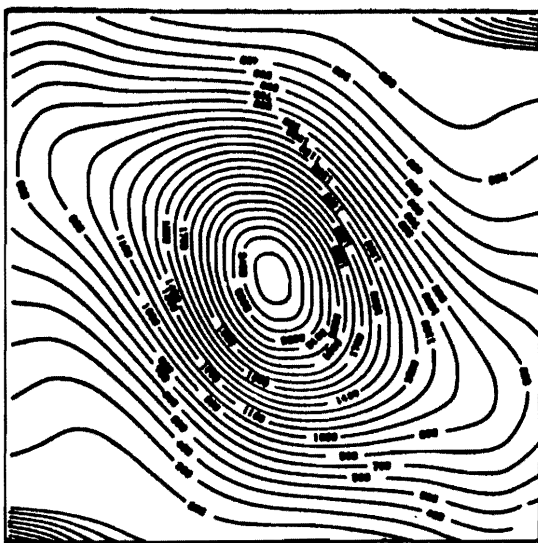


Figure 18. Trend Direction Determined from the Autocorrelogram of the Total Magnetic Vector Map at Interface 0.8 km.

Trans-African NE–SW Trend

This trend was registered as a minor (secondary) direction on all the autocorrelograms of the various versions of the magnetic maps (Figures 11 to 18). Consequently, it might indicate deep-seated as well as near-surface structures.

Ammar and others [20] stated that this trend was registered on the direction frequency histograms of the lineaments as interpreted from both the radiometric and magnetic survey data. Therefore, it could be considered valuable for mineralization of economic importance, including radioactive and magnetic mineralizations.

One of the important observations made from these results is the absence of the Syrian Arc or Qattara trend (ENE–WSW) and the Tethyan or Mediterranean trend (E–W).

According to Anderson's theory of faulting [25], the major axis of the stress ellipsoid is always perpendicular to the main trend, which marks the orientation of planes of rupture which would be a low-angle thrust fault. Besides, the minor (secondary) trends would be the conjugate shear sets for a maximum principal stress oriented perpendicular to the main (principal) trend. Consequently, two maximum principal stresses could be suggested in the area. These are oriented in the ENE (or nearly E–W) and NE directions.

SUMMARY AND CONCLUSIONS

Delineation of geological structures of the area of Kab Amiri, located in the Central Eastern Desert of Egypt, was reached through the application of some integrated interpretation techniques to the data derived from the aeromagnetic survey reduced to the north magnetic pole (RTP). It was proved that the fault zones interpreted from these techniques correlate well with those geologically mapped, or with the linear course of major wadis.

The study proved the existence of several main sets of fault trending in six main directions. These are: the N–S, the NNW–SSE, the Gulf of Suez–Red Sea (NW–SE), the Najd (WNW–ESE), the Gulf of Aqaba (NNE–SSW), and Trans-African (NE–SW) trends. Consequently, the two maximum principal stresses are oriented as follows: ENE (or nearly E–W) and NE.

REFERENCES

- [1] Aero-Service, *Report on Interpretation of Airborne Gamma-Ray Spectrometer and Magnetometer Survey of the Eastern Desert of Egypt, Area IB*. Houston: AeroService, November 1984.
- [2] A. A. Ammar, "Application of Aerial Radiometry to the Study of the Geology of Wadi El Gidami Area, Eastern Desert, Egypt with Aeromagnetic Application", *Ph.D. Thesis, Cairo University, Egypt*, 1973, 424 pp. (Unpublished).
- [3] I. A. El Kassas, "Radioactivity and Geology of Wadi Atalla Area, Eastern Desert", *Ph.D. Thesis, Faculty of Science, Ain Shams University, Egypt*, 1974 (Unpublished).
- [4] F. S. Bakhit, "Geology and Radioactive Mineralization at Jabal El Missikat Area, Central Eastern Desert, Egypt", *Ph.D. Thesis, University of Ain Shams, Cairo, Egypt*, 1978 (Unpublished).
- [5] M. El Shazly, "On the Classification of the Precambrian and Other Rocks of Magnetic Affiliation in Egypt", *Proc. XXII, Int. Geol. Congr.*, Sec. 10, 1964, p. 101.
- [6] M. El Shazly, "Structural Development of Egypt", *Geol. Soc. Egypt, 4th Annual Meeting, Abstracts*, 1966, pp. 31–38.
- [7] M. El Shazly, "The Geology of the Egyptian Region", in *The Ocean Basins and Margins*. ed. A. E. M. Nairn, W. H. Kanes, and F. G. Stehli. Plenum, 1977, pp. 379–444.
- [8] A. H. Sabet, "Geology and Mineral Deposits of Jabal El-Ibai Area, Red Sea Hills, Egypt, UAR", *Ph.D. Thesis, Leiden State University, The Netherlands*, 1961.
- [9] M. Ghanem, "The Geology of Wadi Kareim Area, Eastern Desert, Egypt", *Ph.D. Thesis, Cairo University*, 1968 (Unpublished).
- [10] A. Spector and F. S. Grant, "Statistical Models for Interpreting Aeromagnetic Data", *Geophysics*, **35** (1970), pp. 293–302.
- [11] B. Cianciara and H. Marcak, "Interpretation of Gravity Anomalies by Means of Local Power Spectrum", *Geophysical Prospecting*, **24** (1976), pp. 273–286.
- [12] B. Cianciara and H. Marcak, "Geophysical Anomaly Interpretation of Potential Fields by Means of Singular Points Methods and Filtering", *Geophysical Prospecting*, **27** (1977), pp. 251–260.
- [13] S. I. Rabie and Ahmed A. Ammar, "Delineation of Geological Structures from Aeromagnetic Data Using Some Integrated Interpretation Techniques. El Misikat El Erediya Granitic Plutons, Central Eastern Desert, Egypt", *Egyptian Geophysical Society, Proc. of the 8th Annual Meeting*, March 1990, pp. 111–134.

- [14] R. B. Blackman and J. W. Tukey, *The Measurement of Power Spectra*. New York: Dover Publications, 1959.
- [15] C. W. Horton and others, "A Statistical Analysis of Some Aeromagnetic Maps from the Northwestern Canadian Shield", *Geophysics*, **29(4)** (1964), pp. 582–601.
- [16] W. Domazalski, "Importance of Aeromagnetic in Evaluation of Structural Control of Mineralization", *Geophysical Prospecting*, **14** (1966), pp. 273–291.
- [17] M. S. Reford and J. S. Sumner, "Review Article, Aeromagnetic", *Geophysics*, **29(4)** (1964), pp. 482–516.
- [18] D. S. Parasins, *Mining Geophysics*. Amsterdam, London, New York: Elsevier, 1966.
- [19] M. Krs and others, "Geophysical Phenomena over Deep-Seated Tectonic Zones in Southern Part of Eastern Desert of Egypt", *Annals Geol. Surv. Egypt*, **2** (1973), pp. 125–138.
- [20] A. A. Ammar, M. L. Meleik, and K. M. Fouad, "Tectonic Analysis of a Sample Area, Central Eastern Desert, Egypt, Applying Aeroradiometric and Aeromagnetic Survey Data", *Bull. Fac., Earth Sci., King Abdulaziz University, Jeddah*, **6** (1983), pp. 459–482.
- [21] Samir Riad, "Shear Zones in North Egypt Interpreted from Gravity Data", *Geophysics*, **24(6)** (1977), pp. 1207–1214.
- [22] A. M. A. Gawad, "New Evidence of Transcurrent Movement in Red Sea Area and Petroleum Implications", *Am. Assoc. Pet. Geol. Bull.*, **33** (1969), pp. 1466–1479.
- [23] W. M. Meshref and Mahmoud M. El-Sheikh, "Magnetic Tectonic Trend Analysis in Northern Egypt", *Egypt Geol.*, **17(2)** (1973), pp. 179–184.
- [24] W. M. Meshref, "The Application of Magnetic Trend Analysis to the Interpretation of Egyptian Tectonics", *9th Annual Meeting, Geol. Soc., Egypt, Abstracts*, 1971, pp. 19–21.
- [25] J. Halsey, "Interpretation of Erts Linears", Unpublished Lecture Delivered to Egyptian Geologists in Cairo, 1975.

Paper Received 18 October 1992; Revised 5 April 1993, 22 May 1993; Accepted 14 July 1993.